Computers and Concrete, Vol. 8, No. 1 (2011) 111-123
DOI: http://dx.doi.org/10.12989/cac.2011.8.1.111

Numerical study on concrete penetration/perforation under high velocity impact by ogive-nose steel projectile

Md. Jahidul Islam[1], Zishun Liu*[2] and Somsak Swaddiwudhipong[1]

[1]*Department of Civil Engineering, National University of Singapore, # 1 Engineering Drive 2, Singapore 117576*
[2]*Institute of High Performance Computing, Fusionopolis Way, #16-16 Connexis, Singapore 138632*

(Received September 3, 2009, Accepted January 26, 2010)

Abstract. Severe element distortion problem is observed in finite element mesh while performing numerical simulations of high velocity steel projectiles penetration/perforation of concrete targets using finite element method (FEM). This problem of element distortion in Lagrangian formulation of FEM can be resolved by using element erosion methodology. Element erosion approach is applied in the finite element program by defining failure parameters as a condition for element elimination. In this study strain parameters for both compression and tension at failure are used as failure criteria. Since no direct method exists to determine these values, a calibration approach is used to establish suitable failure strain values while performing numerical simulations of ogive-nose steel projectile penetration/perforation into concrete target. A range of erosion parameters is suggested and adopted in concrete penetration/perforation tests to validate the suggested values. Good agreement between the numerical and field data is observed.

Keywords: high velocity impact; concrete; ogive-nose projectile; perforation; penetration; element erosion.

1. Introduction

Concrete has been used in protective structures for centuries. Because of military interests in resisting projectile and blast impacts, a significant improvement of concrete for protective structure has been observed. Various techniques namely, experimental, analytical and numerical have been developed to predict the resistance of concrete structures under hard projectile impacts. Although more accurate results are obtained from experimental approach with the advent of advanced monitoring instrument, experimental approach has certain drawbacks including high cost and significant amount of time requirement for experimental setup and specimen preparation. These limitations can be resolved by supplementing the experiments with validated numerical approach. Moreover, the latter is able to provide some crucial results which are difficult to obtain from experimental observations. For high velocity impact simulations, several numerical approaches, such as finite element (FE) and mesh free methods are available (Liu *et al.* 2002).

FEM uses two different approaches namely, Eulerian and Lagrangian. Although Eulerian formulation is suitable for large deformation, it suffers from certain disadvantages including difficulties in defining deformable material boundaries and condition of contact between the projectile and the target bodies

* Corresponding author, Ph.D., E-mail: liuzs@ihpc.a-star.edu.sg.

(Camacho and Ortiz 1997). This makes it inapt for ballistic penetration/perforation study. Lagrangian formulation is easier to implement, however, the main challenge in Lagrangian mesh method is in the handling of the large element distortions and damage of target materials. Because of the severe pressure near the projectile nose, elements of the target block undergo large element distortion. Thus, a very small time step is needed leading to the large computational effort followed by a premature termination of the analysis due to negative volume problem. It is necessary to solve the element distortion problem to perform simulation of high velocity penetration/perforation of the projectile.

Schwer and Day (1991) presented several techniques (for example, rezoning, element erosion, tunnel, local modified symmetry constraint and NABOR nodes techniques) to solve the element distortion problem. Among these various approaches element erosion method is widely used because of its simplicity in implementation. It gives a visual representation of the material fracture and damage in numerical analysis which makes it possible to understand material failure in more details for high velocity impact problems. In the element erosion method, severely distorted elements are removed or eroded from further analysis to allow the projectile to penetrate into the target. The elimination process is performed based on some failure criteria such as, maximum or minimum pressures, stresses or strains. However, there is no test procedure available to determine these failure criteria for an intended target material. To determine the erosion parameters, a calibration method is used with certain experimental results.

Holmquist *et al.* (1993) performed perforation study of the concrete block with compressive strength of 48 MPa using a two-dimensional (2D) computational approach. The results were in good agreement with the experimental data performed by Hanchak *et al.* (1992). However, the element distortion problem or the failure criteria were not mentioned. Chen (1993) carried out the perforation study on 140 MPa strength concrete using a 2D axisymmetric approach in LS-DYNA2D and compared the residual velocities with those measured by Hanchak *et al.* (1992). For concrete, Chen (1993) used the strain values of 0.15 and 1.0 as a failure criterion in the erosion algorithm along with the material model for compression and tension failure, respectively. Polanco-Loria et al. (2008) performed 2D axisymmetric perforation study of both the 48 MPa and 140 MPa concretes (Hanchak *et al.* 1992) in LS-DYNA, and a used failure strain value of 1.0. Furthermore, in a 2D axisymmetric finite element analysis of ogive nose steel projectile penetration into concrete with unconfined compressive strength of 43 MPa, Johnson *et al.* (1998) simulated the penetration of the projectile with striking velocity of 315 m/s by using an erosion strain value of 3.0. Beissel and Johnson (2000) also chose a similar value for erosion while carrying out a 2D axisymmetric penetration of concrete by ogive-nose steel projectile in a Lagrangian hydrocode. Although these numerical results were in good agreement with the experimental data, a wide range of erosion parameter values were used for different perforation/penetration cases and none of them were consistent. Therefore, further studies are required to find a consistent set of failure parameters which can be used for ogive-nose projectiles penetration/ perforation problems of concrete targets.

2. Element erosion

Element erosion technique is implemented to eliminate the highly distorted elements which exist in front of and around the projectile nose for further analysis during penetration/perforation of the

projectile. It should be noted that the element erosion is a numerical consideration and not as same as the material failure. In this method, the elimination process is performed by the use of element removal criteria usually related to pressure, stress or strain of elements. When the condition satisfy the erosion criteria, element stress states become void and the element removed from subsequent analysis.

Element erosion approach can be either applied with the material constitutive model or as a separate option. Since most of the constitutive models do not contain erosion, a separate option where erosion criteria can be set independently is the preferred alternative. Some of the most familiar independent failure criteria for element erosion are shown as follows

$$P \geq P_{max} \tag{1}$$

$$P \leq P_{min} \tag{2}$$

$$\sigma_1 \geq \sigma_{max} \tag{3}$$

$$\sqrt{\frac{3}{2}\sigma_{ij}^{'}\sigma_{ij}^{'}} \geq \overline{\sigma} \tag{4}$$

$$\varepsilon \geq \varepsilon_{max} \tag{5}$$

$$\varepsilon \leq \varepsilon_{min} \tag{6}$$

Eqs. (1) and (2) are pressure erosion criteria. In which, P is the pressure; P_{max} and P_{min} are the maximum and minimum pressure at failure. For stress erosion criteria, the failure stress can be either the maximum principal stress or the equivalent stress as shown in Eqs. (3) and (4). Where, σ_1 is the maximum principal stress, σ_{max} is the maximum principal stress at failure, $\sigma_{ij}^{'}$ is the deviatoric stress and $\overline{\sigma}$ is the equivalent stress at failure. Moreover, Eqs. (5) and (6) give the strain erosion criteria where, ε is the strain, and ε_{max} and ε_{min} are the maximum and minimum principal strains at failure. Among all these criteria, strain based element erosion criteria is the most popular (Chen 1993, Polanco-Loria *et al.* 2008, Johnson *et al.* 1998, and Beissel and Johnson 2000). Therefore, in this present study, the strain erosion criterion is used as an element erosion criterion for concrete penetration/perforation by a steel projectile.

When a hard projectile impacts on a concrete target, a compressive wave is created at the contact surface and propagates along the target towards the other surface. Once the compressive wave reaches the free surface it reflects back as a tensile wave (Gebbeken and Ruppert 2000). If stresses generated by these waves are larger than the compressive/tensile strength of the concrete, fracture and fragmentation of concrete could occur. Therefore, in numerical studies of concrete penetration/perforation, both tensile and compressive failure criteria in the element erosion should be considered.

In the present study, maximum and minimum principal strains at failure as mentioned in Eqs. (5) and (6) have been chosen as the element erosion criteria. Since these strains values are unknown and there are no direct methods available to determine these values, a calibration approach is adopted to establish these parameters. A wide range of strains at failure parameters are used in numerical simulations while other parameters and conditions remain unchanged. A set of strains at failure values is chosen based on the correlation with available experimental data. The same set of failure values is then verified based on other experimental results.

3. Numerical simulations

When concrete is subjected to high velocity impact it undergoes high pressures, large strains, high strain rates and damage. Therefore, it is necessary to use a material model which includes these effects in constitutive conditions. In the present study, Holmquist-Johnson-Cook (HJC) material model for concrete (Holmquist *et al.* 1993) is used to model the concrete targets. The HJC is an elastic-plastic damage model which considers high strain, strain rate effects and damage.

In the HJC (Holmquist *et al.* 1993) model, the normalized equivalent stress is defined as

$$\sigma_{eq}^{*} = \frac{\sigma_{eq}}{f_c'} = [A(1-D)+BP^{*N}]\left[1+C\ln\left(\frac{\dot{\varepsilon}}{\dot{\varepsilon}_0}\right)\right] \le S_{max} \tag{7}$$

Where, σ_{eq} is the equivalent stress, f_c' is the unconfined compressive strength of concrete, $P^{*} = P/f_c'$ is the normalized pressure, P is the current pressure, $\dot{\varepsilon}$ is the current and $\dot{\varepsilon}_0$ is the reference strain rate. In Eq. (7), normalized cohesive strength A, normalized pressure hardening coefficient B, strain rate coefficient C, pressure hardening exponent N, and normalized maximum strength S_{max} are all material constants. Material damage has also been incorporated using a damage variable D. Stress-pressure relationship of the material model is presented in Fig. 1.

The HJC model uses a strain based damage model, where damage D $(0 \le D \le 1)$ is calculated from both incremental equivalent plastic strain $(\Delta\varepsilon_p)$ and incremental equivalent plastic volumetric strain $(\Delta\mu_p)$ and expressed as

$$D = \sum \frac{\Delta\varepsilon_p + \Delta\mu_p}{\varepsilon_p^f + \mu_p^f} \tag{8}$$

Where, the plastic strain to fracture $\varepsilon_p^f + \mu_p^f$ can be defined as

$$\varepsilon_p^f + \mu_p^f = D_1(P^{*} + T^{*})^{D_m} \ge \varepsilon_{min}^f \tag{9}$$

D_1 and D_m are the damage constants and $T^{*} = T/f_c'$ is the normalized maximum tensile strength. This plastic strain to fracture value is limited by an additional damage constant ε_{min}^f in order to limit the plastic strain for material fracture. Damage response of the material model is plotted in Fig. 2(a).

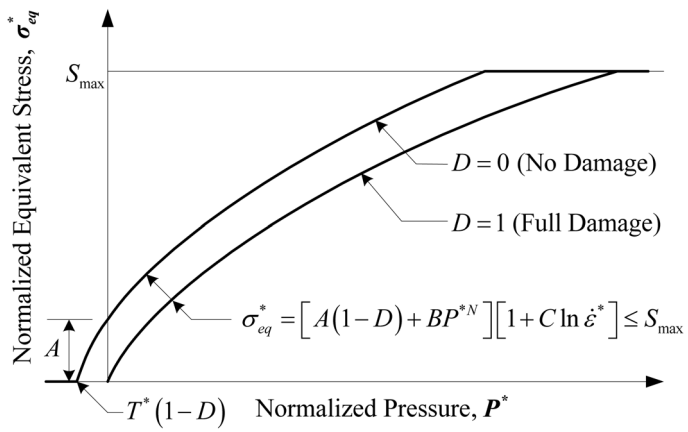

Fig. 1 Shear-pressure response of the HJC concrete model (after Holmquist *et al.* 1993)

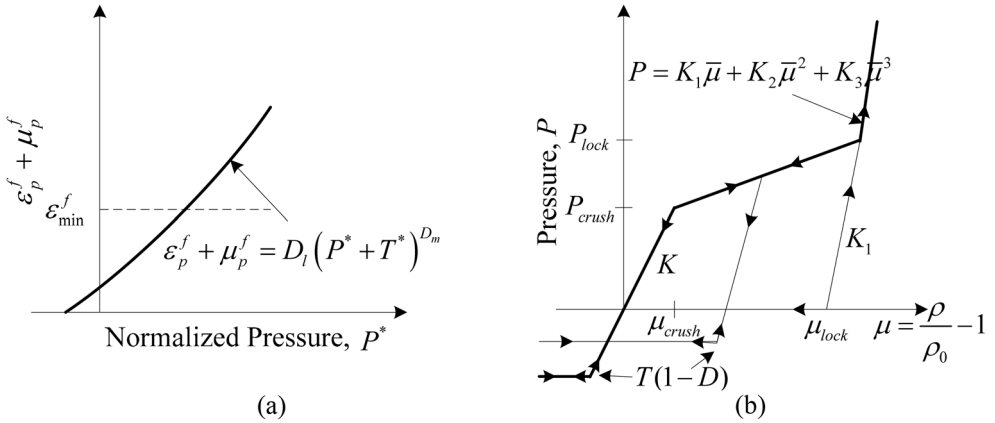

Fig. 2 Damage and pressure-volume responses of the HJC concrete model (after Holmquist *et al.* 1993)

The pressure-volume behavior of HJC concrete model can be expressed in three regions (Fig. 2(b)). The linear elastic part is limited by the pressure and volumetric strain values of P_{crush} and μ_{crush}, respectively. In the transition region between the elastic and the total damaged concrete, the material undergoes damage with the presence of plastic volumetric strain. The region ranges from the pressure values P_{crush} to P_{lock}. At the end of this region, it is assumed that the material is totally damaged and compacted with no tensile strength. The third region defines the fully dense material without any air voids and the pressure-volume responses at this region is expressed as

$$P = K_1\bar{\mu} + K_2\bar{\mu}^2 + K_3\bar{\mu}^3 \tag{10}$$

K_1, K_2 and K_3 are the material constants, $\bar{\mu} = (\mu - \mu_{lock})/(1 + \mu_{lock})$ is the modified volumetric strain, $\mu = \rho/\rho_0 - 1$ is the standard volumetric strain (where, ρ is the current density and ρ_0 is the initial density) and $\mu_{lock} = \rho_{grain}/\rho_0 - 1$ is the locking volumetric strain (where, ρ_{grain} is the grain density). Material properties of the HJC concrete model for plain concrete with compressive strength of 48 MPa are listed in Table 1.

The HJC concrete model does not have the element erosion option and the latter option is adopted separately along with the material model. Both compression and tension strains at failure are used as erosion criteria in the element erosion option. The present study covers the compression strain values at failure ranging from -0.4 to -1.2; and those associated with tension failure from 0.2 to 1.0.

For the steel projectile material modeling, a simple elastic-plastic material model is used. As the projectile deformation is expected to be minimal except for limited erosion near the projectile nose, a strain failure value is also adopted as an element erosion criterion in the constitutive model for the

Table 1 Material properties of HJC concrete model for 48 MPa concrete (Holmquist *et al.* 1993)

ρ_0 (kg/m^3)	E (GPa)	ν	G (GPa)	T (MPa)	ε_{min}^f	
2440	35.7	.2	14.86	4	0.01	
A	B	N	C	S_{max}	D_l	D_m
0.79	1.60	0.61	0.007	7.0	0.04	1.0
P_{crush} (GPa)	μ_{crush}	P_{lock} (GPa)	μ_{lock}	K_1 (GPa)	K_2 (GPa)	K_3 (GPa)
0.016	0.001	0.80	0.1	85	-171	208

steel projectile.

Numerical analysis has been performed in dynamic hydrocode LS-DYNA. To reduce computational effort, a fixed mesh of 4-node two-dimensional (2D) axisymmetric elements (y-axis of symmetry) is used for both projectile and target. Hourglass option is used to reduce the spurious zero energy modes. To define the conditions of contact between the steel projectile and the concrete target, a 2D automatic_surface_to_surface contact option is used for all cases. Although, the projectiles showed some pitch and yaw in the experiment, they were significantly below the critical level and all the projectile impacts in the numerical models are considered normal impact in the current study.

Two perforations and one penetration tests of concrete with compressive strength of 48 MPa, 140 MPa and 62.8 MPa, respectively are used to establish the erosion parameters. Hanchak *et al.* (1992) conducted two projectile perforation tests into concrete targets. In the perforation experiments, 48 MPa and 140 MPa concrete slabs with dimension of 610×610×178 mm^3 were impacted by 25.4 mm diameter ogive-nose maraging steel (T-250) projectiles at striking velocity ranging from 300 m/s to 1100 m/s. The residual velocities of the projectiles obtained in the experiments were plotted against the initial projectile velocities. Other test includes the penetration test of the 20.3 mm diameter ogive-nose 4340 steel projectile into 62.8 MPa concrete (Forrestal *et al.* 1996) targets of cylindrical in shape with a diameter of 0.51 m and the length varying from 0.91 m to 1.83 m. The striking

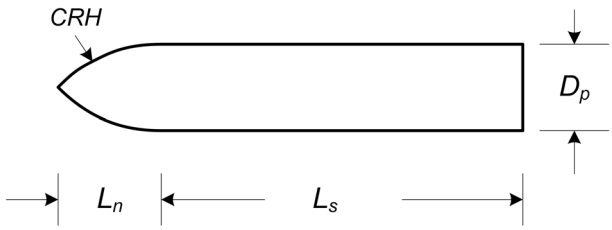

Fig. 3 A typical ogive-nose projectile geometry (CRH-caliber-radius-head)

Table 2 Properties of concrete target and steel projectile

	Perforation (Hanchak *et al.* 1992)		Penetration (Forrestal *et al.* 1996)		Penetration (Frew *et al.* 1998)	
Concrete target						
f_c' (MPa)	48.0	140.0	62.8	51.0	58.4	58.4
ρ_0 (kg/m^3)	2440	2520	2300	2300	2320	2320
Target dia (mm)	610	610	510	910	510	910
Target length (m)	0.178	0.178	0.91-1.52	1.83-2.74	0.94-1.93	1.07-3.05
Steel projectile						
Mass, m (kg)	0.50	0.50	0.48	1.60	0.478	1.62
Density, ρ_0 (kg/m^3)	8020	8020	7850	7850	7850	7850
Yield stress, σ_Y (GPa)	1.72	1.72	1.45	1.45	1.45	1.45
Shank dia., D_p (mm)	25.4	25.4	20.3	30.5	20.3	30.5
Shank length, L_s (mm)	101.6	101.6	169.5	254.3	169.5	254.2
Nose length, L_n (mm)	42.1	42.1	33.7	50.5	33.7	50.5
Caliber-radius-head	3	3	3	3	3	3

velocities of the projectile were varied from 450 m/s to 1224 m/s. A typical ogive-nose projectile is illustrated in Fig. 3; whereas, dimensions and properties of the concrete targets and the steel projectiles are given in Table 2. Penetration depths of the projectiles were measured for various initial projectile velocities.

Three other penetrations of concrete by ogive-nose steel projectile tests are considered for the verification of the erosion parameters. The first one is the penetration study of 30.5 mm ogive-nose 4340 steel projectile into 0.91 m diameter concrete target with unconfined compressive strength of 51.0 MPa (Forrestal *et al.* 1996), and initial projectile velocities varying from 405 m/s to 1201 m/s. The other two are the penetration studies of 20.3 mm and 30.5 mm ogive-nose 4340 steel projectiles into 0.51 m and 0.91 m diameter concrete targets with unconfined compressive strength of 58.4 MPa (Frew *et al.* 1998), and initial projectile velocities varying from 440 m/s to 1176 m/s and 1.07 m to 3.05 m, respectively.

4. Results and discussions

In order to perform the mesh sensitivity study, a uniform mesh is used in the concrete target domain along the path of the projectile and the rest of the domain is modeled with gradually coarser mesh towards the boundary. For the uniform mesh region, three different mesh sizes are chosen, 1 mm × 1 mm, 2 mm × 2 mm and 4 mm × 4 mm. Two cases are selected, (i) the perforation of 48 MPa concrete (Hanchak *et al.* 1992) and (ii) the penetration of 62.8 MPa concrete (Forrestal *et al.* 1996). The residual velocities and the penetration depths against the initial velocities of the projectile for 48 MPa and 62.8 MPa concretes with three mesh sizes are plotted in Fig. 4 and 5 respectively. A mesh convergence is achieved with a mesh size of 2 mm × 2 mm for both cases and adopted in subsequent studies. Fig. 6 shows the mesh of the projectile and the target for the perforation test of 48 MPa concrete.

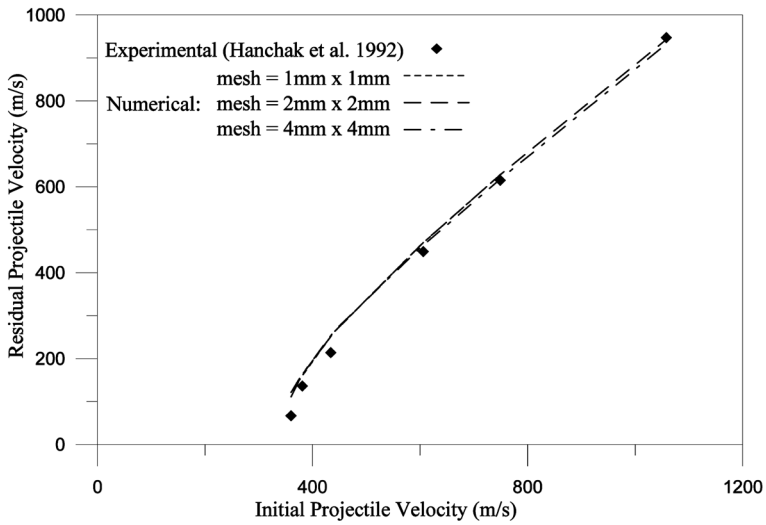

Fig. 4 Comparison of projectile residual velocities against initial velocities in the perforation test of 48 MPa concrete with varying mesh size

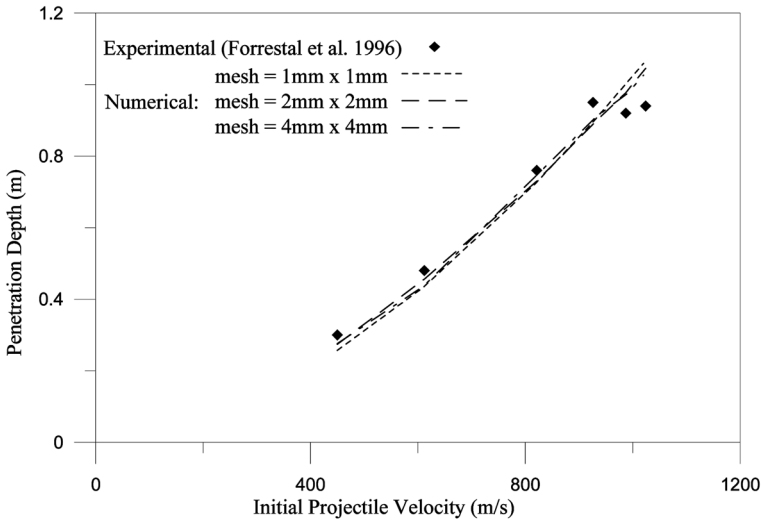

Fig. 5 Comparison of projectile penetration depths against initial velocities in the penetration test of 62.8 MPa concrete with varying mesh size

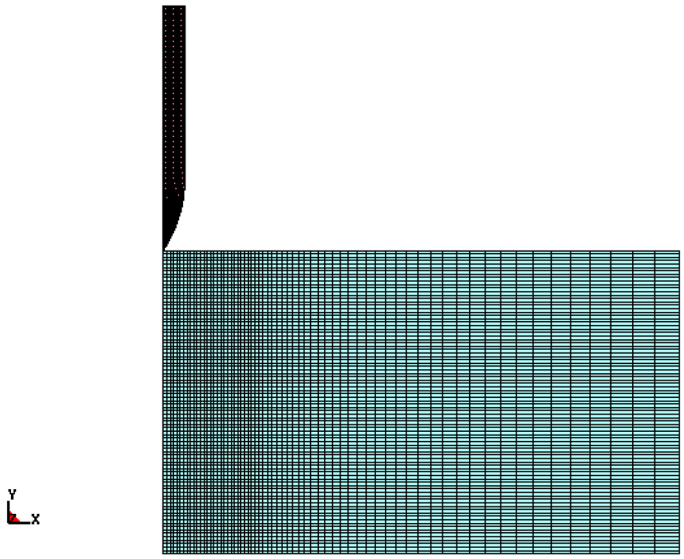

Fig. 6 A typical mesh of the projectile and the target

The residual velocities and the penetration depths of the projectile from the perforation and penetration tests respectively are adopted in the calibration of the erosion parameters. The root mean square error (RMSE) is evaluated using the following expression

$$RMSE = \sqrt{\frac{1}{n}\sum_{n=1}^{n}\left(\frac{(Exp)_n - (Num)_n}{(Exp)_n}\right)^2} \tag{11}$$

Here, n is the number of points, Exp is the observed experimental data and Num is the numerical

Table 3 RMSE for various tfs and cfs (Shaded portion encompass the desirable range)

		Root mean square error (RMSE)		
tfs	cfs	Perforation (f_c' = 48 MPa)	Perforation (f_c' = 140 MPa)	Penetration (f_c' = 62.8 MPa)
0.2	-0.5	0.649	0.227	0.271
0.2	-0.7	0.659	0.228	0.252
0.2	-0.8	0.659	0.228	0.252
0.2	-1.0	0.668	0.228	0.252
0.2	-1.2	0.659	0.228	0.252
0.3	-0.5	0.617	0.094	0.219
0.3	-0.7	0.551	0.046	0.200
0.3	-0.8	0.579	0.046	0.195
0.3	-1.0	0.552	0.046	0.194
0.3	-1.2	0.579	0.046	0.195
0.4	-0.5	0.618	0.095	0.216
0.4	-0.7	0.341	0.189	0.072
0.4	-0.8	0.297	0.037	0.073
0.4	-1.0	0.311	0.198	0.077
0.4	-1.2	0.280	0.198	0.077
0.5	-0.5	0.619	0.108	0.212
0.5	-0.7	0.345	0.099	0.079
0.5	-0.8	0.262	0.104	0.082
0.5	-1.0	0.283	0.381	0.087
0.5	-1.2	0.314	0.058	0.091
0.7	-0.5	0.620	0.107	0.215
0.7	-0.7	0.330	0.149	0.080
0.7	-0.8	0.336	0.240	0.086
0.7	-1.0	0.050	0.164	0.142
0.7	-1.2	0.088	0.450	0.147
1.0	-0.5	0.618	0.099	0.219
1.0	-0.7	0.348	0.143	0.079
1.0	-0.8	0.312	0.448	0.085
1.0	-1.0	0.110	0.098	0.156
1.0	-1.2	0.084	0.450	0.166

results. Table 3 shows the root mean square errors for three different cases of concrete perforation/ penetration for various combinations of tensile failure strain (tfs) and compressive failure strain (cfs) values. It is observed that a range of tfs values of 0.4 to 0.5 and cfs values of -0.8 to -1.0 provide results that are in good agreement with the test values as illustrated in Figs. 7 and 8. As the variation of numerical results is minimal, it is suggested that the tfs value of 0.5 and cfs value of -1.0 are adopted for the subsequent analyses. Projectile residual velocities plotted against the projectile initial velocities for high strength concrete (f_c' = 140 MPa) are illustrated in Fig. 9, shown a good correlation with the test data.

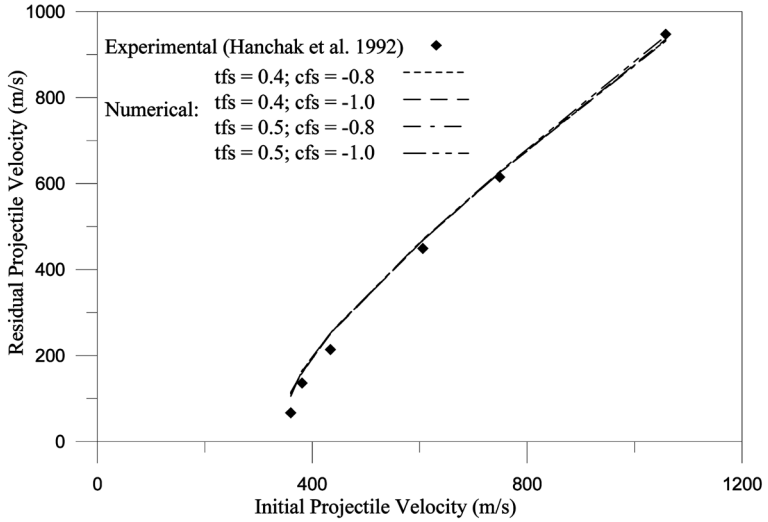

Fig. 7 Comparison of projectile residual velocities against initial velocities in the perforation test of 48 MPa concrete with varying tfs and cfs

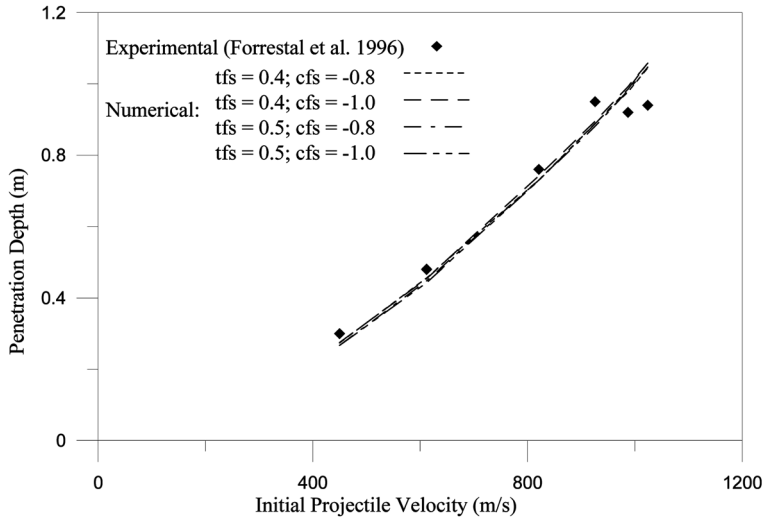

Fig. 8 Comparison of projectile penetration depths against initial velocities in the penetration test of 62.8 MPa concrete with varying tfs and cfs

In the perforation experiment, Hanchak *et al.* (1992) observed conical crater regions at both top and bottom surfaces and a cylindrical tunnel region in the middle portion. Fig. 10 displays the concrete target after perforation by the projectile at a striking velocity of 749 m/s. The missing elements along the path of the projectile have been eroded from the analysis. It shows a tunnel region in between the top and bottom crater regions. It is observed that the conical top and bottom crater regions occur mostly due to the compressive and tensile waves involving in the impact process; whereas, the tunnel region forms when the projectile passes through the target by removing the elements in front of the projectile and the latter has a diameter similar to the diameter of the

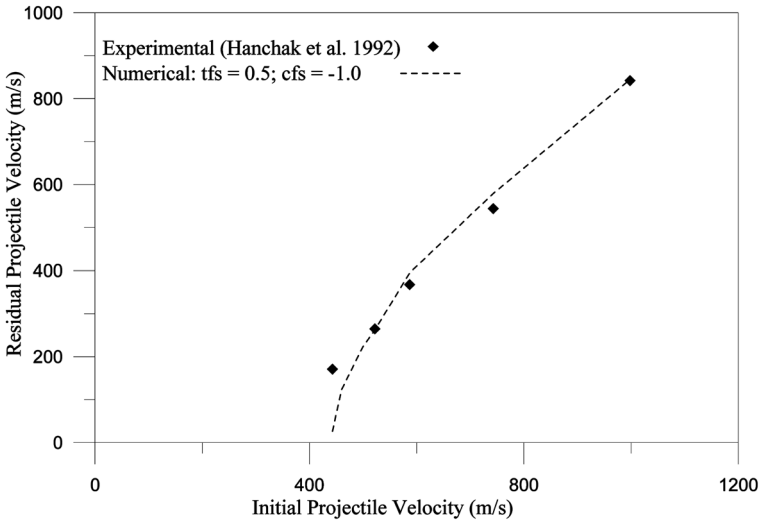

Fig. 9 Comparison of projectile residual velocities against initial velocities in the perforation test of 140 MPa concrete

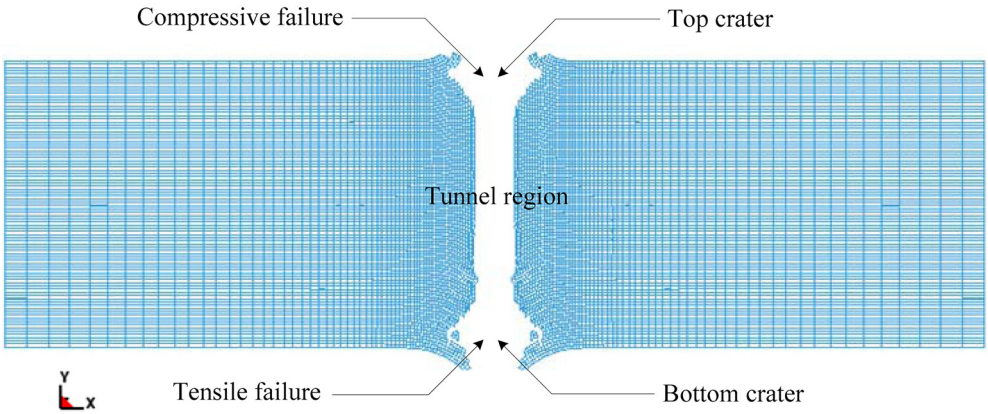

Fig. 10 Concrete target after perforation of 48 MPa concrete with initial velocity of 749 m/s

projectile. This indicates that the numerical approach with element erosion is able to recapture the failure patterns observed in the experiment.

Three other penetration cases are used herein to verify the selected erosion parameters (tfs = 0.5 and cfs = -1.0). The first example is the penetration of the 30.5 mm diameter ogive-nose steel projectile into the 51.0 MPa concrete target (Forrestal *et al.* 1996). The comparison of numerically obtained penetration depths with the experimental data are plotted in Fig. 11. The other two cases are from Frew *et al.* (1998), where ogive-nose steel projectiles with diameter of 20.3 mm and 30.5 mm are penetrated into 58.4 MPa concrete targets. Once again, Fig. 12 demonstrates that the numerical results are in good agreement with experimental results.

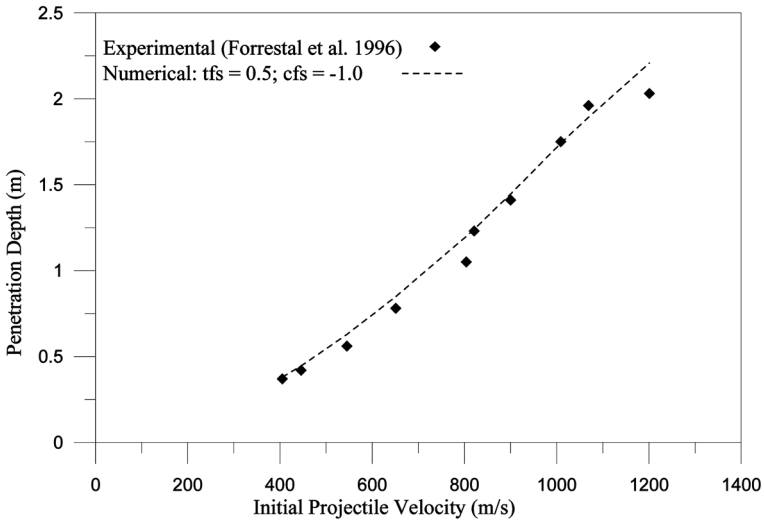

Fig. 11 Comparison of penetration depths against initial velocities for the 51.0 MPa concrete penetration test with projectile diameter of 30.5 mm

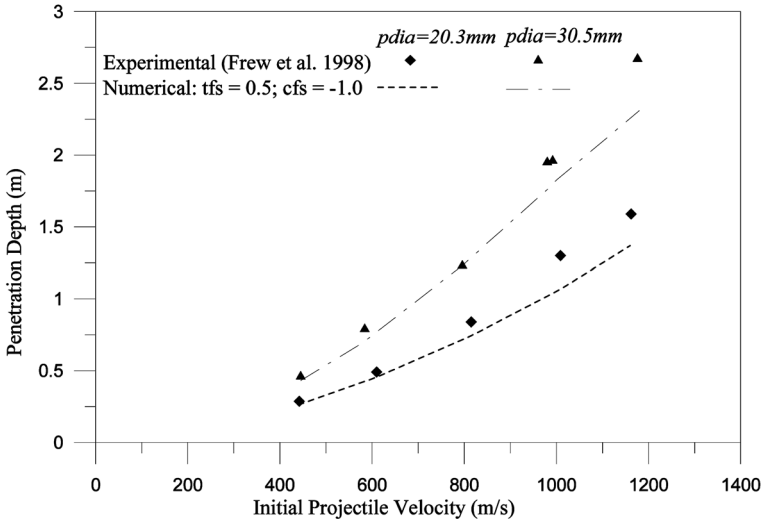

Fig. 12 Comparison of penetration depths against initial velocities for the 58.4 MPa concrete penetration tests with projectile diameter (pdia) of 20.3 and 30.5 mm

5. Conclusions

Numerical analyses of penetration and perforation of concrete targets by high velocity ogive-nose steel projectiles are presented in this study. Severe element distortion problem is mitigated by the use of the element erosion method. Strain values of 0.5 and -1.0 are selected as failure criteria for tension and compression failure, respectively. These values are verified with other published experimental results. It is noted that the failure patterns of concrete targets obtained numerically

resemble those observed experimentally. The approach as presented herein adopts a consistent set of values of material properties and numerical parameters covering both the penetration and perforation of steel projectiles with ogive-nose into concrete targets with unconfined compressive strength of 48 MPa to 140 MPa.

References

Beissel, S.R. and Johnson, G.R. (2000), "An abrasion algorithm for projectile mass loss during penetration", *Int. J. Impact Eng.*, **24**, 103-116.

Camacho, G.T. and Ortiz, M. (1997), "Adaptive Lagrangian modeling of ballistic penetration of metallic targets", *Comput. Method. Appl. Mech. Eng.*, **142**, 269-301.

Chen, E.P. (1993), *Numerical simulation of perforation of concrete targets by steel rods*, Advances in Numerical Simulation Techniques for Penetration and Perforation of Solids, ASME, **AMD171**, 181-188.

Forrestal, M.J., Frew, D.J., Hanchak, S.J. and Brar, N.S. (1996), "Penetration of grout and concrete targets with ogive-nose steel projectiles", *Int. J. Impact Eng.*, **18**(5), 465-476.

Frew, D.J., Hanchak, S.J., Green, M.L. and Forrestal, M.J. (1998), "Penetration of concrete targets with ogive-nose steel rods", *Int. J. Impact Eng.*, **21**(6), 489-497.

Gebbeken, N. and Ruppert, M. (2000), "A new material model for concrete in high-dynamic hydrocode simulations", *Arch. Appl. Mech.*, **70**, 463-478.

Hanchak, S.J., Forrestal, M.J., Young, E.R. and Ehrgott, J.Q. (1992), "Perforation of concrete slabs with 48 MPa (7 ksi) and 140 MPa (20 ksi) unconfined compressive strengths", *Int. J. Impact Eng.*, **12**(1), 1-7.

Holmquist, T.J., Johnson, G.R. and Cook, W.H. (1993), "A computational constitutive model for concrete subjected to large strains, high strain rates, and high pressures", *Proceedings of Fourteenth International Symposium on Ballistics*, Quebec City, Canada, September, 1-10.

Johnson G.R., Beissel S.R., Holmquist T.J. and Frew D.J. (1998), "Computed radial stresses in a concrete target penetrated by a steel projectile", In: Jones, N., Talaslidis, D.G., Brebbia, C.A., Manolis, G.D. (Eds.), *Structures Under Shock and Impact V*, Computational Mechanics Publications, 793-806.

Liu, Z.S., Swaddiwudhipong, S. and Koh, C.G. (2002), "Stress wave propagation in 1-D and 2-D media using smooth particle hydrodynamics method", *Struct. Eng. Mech.*, **14**(4), 455-472.

Polanco-Loria, M., Hopperstad, O.S., Børvik, T. and Berstad, T. (2008), "Numerical predictions of ballistic limits for concrete slabs using a modified version of the HJC concrete model", *Int. J. Impact Eng.*, **35**(5), 290-303.

Schwer, L.E. and Day, J. (1991), "Computational techniques for penetration of concrete and steel targets by oblique impact of deformable projectiles", *Nuclear Eng. Des.*, **125**, 215-238.